RSC Advances

Check for updates

Highly permeable and stable forward osmosis (FO) membrane based on the incorporation of Al₂O₃ nanoparticles into both substrate and polyamide active layer†

Wande Ding,[ab] Yiming Li,[ab] Mutai Bao, [iD] *[ab] Jianrui Zhang,[ab] Congcong Zhang[ab] and Jinren Lu[b]

In the present study, hydrophilic Al₂O₃ nanoparticles were used as additives in both substrate and polyamide active (PA) layer to improve forward osmosis (FO) membrane properties. *Via* incorporation of 0.5 wt% Al₂O₃ into the substrate and 0.05 wt% Al₂O₃ into the PA layer (PS$_{0.5}$-TFN$_{0.05}$ membrane), the water flux reached 27.6 L m^{-2} h^{-1} with a relatively low solute reverse flux of 7.1 g m^{-2} h^{-1} using DI water as a feed solution and 1 M NaCl as a draw solution. Simultaneously, we found that the incorporation of Al₂O₃ nanoparticles into both the substrate and PA layer resulted in a better enhancement of FO performance and a higher increase in water flux than the simple incorporation of nanoparticles in substrate. Moreover, the PS$_{0.5}$-TFN$_{0.05}$ membrane remained stable during long-term FO tests and under serious water environment. To the best of our knowledge, this is the first study to report the effect of Al₂O₃ nanoparticles on FO performance, and the results verify the potential use of these nanoparticles in the fabrication of highly permeable FO membranes.

1. Introduction

Over the past few decades, the emergence of forward osmosis (FO) has attracted significant attention in membrane technology as FO is a potential cost-effective desalination process in addressing the shortage of water scarcity worldwide.[1,2] Driven by osmotic pressure difference across the FO membrane, water molecules can freely pass through the membrane from the low osmosis pressure side to the high osmosis pressure side, whereas the solutes are retained.[3,4] Low energy consumption,[5] reduced fouling tendency,[6] and high water recovery of FO process make it one of the most promising water purification and desalination technologies in energy generation, water supply, and food processing.[7-9] However, the main obstacle in FO process is internal concentration polarization (ICP), which limits the performance of FO membranes.[10-12] In general, dilutive ICP occurs when the active layer faces the feed solution (AL-FS) as a result of draw solute dilution around the support layer and accumulation of the feed solutes around the rejection layer. When the active layer faces the draw solution (AL-DS), the rejected feed solutes accumulate in the support layer, resulting

in concentrative ICP.[5] Both dilutive and concentrative ICP may cause reduction in effective osmotic pressure across the membrane, which induces a low water flux.[13] It is generally agreed that to minimize the ICP effect on FO process, a small structural parameter S (S = thickness × tortuosity/porosity) is used for the support layer.[14] Therefore, an ideal FO membrane should consist of (1) an active layer with high water permeability and low solute permeability and (2) a support layer with smaller structural parameters such as lower tortuosity, higher porosity, and thinner thickness.

Recently, addition of nanomaterials in substrate or polyamide active (PA) layer of thin-film composite (TFC) and thin film nanocomposite (TFN) FO membrane has emerged as a research hotspot for improving membrane properties. The majority of filled porous materials are inorganic nanoparticles, such as zeolite,[15,16] mesoporous silica,[17] carbon nanotubes[18] and metal organic frameworks (MOFs).[19] These nanomaterials with porous structure and hydrophilic nature could effectively improve substrate properties (porosity, pore size and hydrophilicity), as well as establish direct water channels in the dense PA layer for fast transportation of water molecules, leading to increasing water permeance of membranes.[5] Emadzadeh *et al.*[1] first reported a decreased S value by adding TiO₂ nanoparticles in a PSf substrate. The reduction of S value indicated effective inhibition of ICP in FO performance, which contributed to considerable increase in water flux of the resultant FO membrane. Ma *et al.*[10] investigated the influence of zeolite on

[a]Key Laboratory of Marine Chemistry Theory and Technology, Ministry of Education, Ocean University of China, Qingdao 266100, China. E-mail: mtbao@ouc.edu.cn

[b]College of Chemistry & Chemical Engineering, Ocean University of China, Qingdao 266100, China

FO performance by incorporating porous zeolite nanoparticles in PS substrate. Enhanced water flux was achieved using PS-zeolite substrate with a lower S value (0.34 mm) compared to that of TFC membrane prepared on a conventional PS substrate (S value was 0.96 mm). Similar results were also reported by other groups.[20,21] Instead of incorporating nanomaterials in substrate, Niksefat et al.[17] added silica nanoparticles in PA layer to improve FO membrane performance. They observed that water flux of TFN membranes was nearly 2 times higher than that of TFC membranes with 0.05 w/v% silica addition in PA layer. Besides, by dispersion of multi-walled carbon nanotubes in PA layer, Amini et al.[5] also obtained a great enhancement in water flux of TFN membranes. All the results demonstrated that incorporation of nanomaterials in substrate or PA layer was an effective method to fabricate highly permeable FO membranes. Despite the significant achievements in nanomaterial-based FO membranes, there is still an urgent need for seeking for new nanomaterials to prepare high-performance membranes with enhanced water flux and improved salt rejection for good water quality.

Al$_2$O$_3$ nanoparticles have been widely used in various fields such as adsorbents, composite materials,[22,23] and membrane preparation,[24,25] because they possess many advantages such as high surface area, large pore volume[26] and high porosity.[27] Furthermore, a cheaper price compared to CNTs, TiO$_2$ and MOFs is also an attractive point. Yan et al.[24] fabricated Al$_2$O$_3$–PVDF composite membranes by addition of Al$_2$O$_3$ nanoparticles in PVDF ultrafiltration membrane, and they showed a great improvement in water flux and anti-fouling performance. Saleh et al.[28] studied the effect of Al$_2$O$_3$ nanoparticles on reverse osmosis performance by incorporating them in PA layer, and both water flux and salt rejection exhibited an obvious elevation. These observations suggested that Al$_2$O$_3$ nanoparticles are of great potential for preparation of membranes with excellent separation performance. However, it has been observed that there is no report on the effect of Al$_2$O$_3$ nanoparticles on FO performance until now.

In view of this, the main objective of this work is to investigate the effects of Al$_2$O$_3$ nanoparticles on the FO performance upon their addition in PS substrate as well as PA layer. The proposed membrane structure between Al$_2$O$_3$ nanoparticles and polymer matrix is schematically depicted in Fig. 1. We first prepared two types of substrates, PS and PS-Al$_2$O$_3$, followed by the observation of property changes of the PS substrate. We further incorporated Al$_2$O$_3$ nanoparticles onto PA layer via

interfacial polymerization and investigated the new layer by SEM, EDX, porosity and AFM characterization. Then, we conducted FO test to evaluate water flux and solute reverse flux, as well as membrane stability.

2. Experimental

2.1 Materials

Polysulfone (PS-3500P) was obtained from Solvay Advanced Polymers (Belgium). m-Phenylenediamine (MPD) and trimesoyl chloride (TMC) were purchased from Sigma-Aldrich (USA). Commercial aluminum oxide nanoparticles (<50 nm, γ-Al$_2$O$_3$, Sigma-Aldrich, USA) were used as additives in substrate and PA layer. A commercial polyester mesh (PE mesh, thickness ∼90 μm) was provided from Hebei Crane Achieves Network Industry Co., Ltd (China) and used as a backing layer for the substrate. Sodium chloride (NaCl) was used to prepare the draw solution and obtained from BASF chemical industry (China). Polyethylene glycol ($M_w = 400$) was obtained from Sinopharm Chemical Reagent Co. Ltd., China. Other materials were of the highest available purity and used without further purification. Milli-Q water (Millipore), with a resistivity of 18.2 MΩ cm, was used to prepare various solutions and for FO measurements.

2.2 Flat sheet TFC and TFN FO membranes

2.2.1 Preparation of PS and PS-Al$_2$O$_3$ substrates. The substrates were synthesized by using a phase-inversion method.[18,29] The compositions of dope solutions are listed in Table 1. In brief, certain amounts of PS, PEG and LiCl were dissolved in DMAc. Then the dope solution was stirred using a magnetic stirrer for 24 h at 70 °C. After that, the resulting homogeneous dope solution was stored at room temperature for more than 24 h to remove air bubbles trapped within it. To prepare PS-Al$_2$O$_3$ substrate, 0.5 wt% Al$_2$O$_3$ nanoparticles were first added to the DMAc/PEG/LiCl mixed solution, followed by a 30 min ultra-sonication to minimize agglomeration. Soon after, PS beads were dissolved in the mixed solution system and the abovementioned procedure was repeated. Afterwards, the resulting homogeneous dope solution was spread over polyester mesh using an in-house casting device to form 90 μm mesh-embedded substrates. Finally, the resultant substrates were stored in a DI water bath for at least 24 h before use. The substrate with 0.5 wt% Al$_2$O$_3$ nanoparticles was denoted as PS$_{0.5}$.

2.2.2 Preparation of TFC and TFN membranes. TFC and TFN membranes were formed by an interfacial polymerization
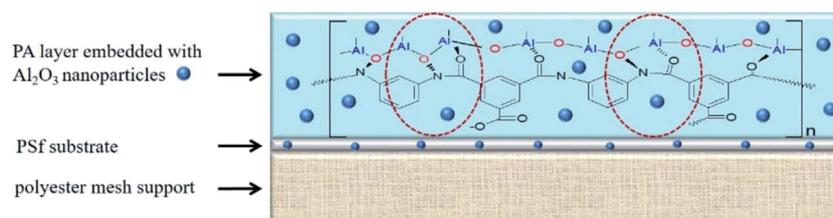

Fig. 1 Structure and mechanism of Al$_2$O$_3$ nanoparticles embedded in the membrane by coordination between Al$_2$O$_3$ nanoparticles and polymer matrix.

Table 1 Synthesis conditions for substrate, TFC and TFN membranes

Membrane	Composition of dope solution					Composition of aqueous and organic solution during IP		
	PS (wt%)	PEG (wt%)	LiCl (wt%)	DMAc (wt%)	Al_2O_3 (wt%)	MPD (wt/v%)	TMC (wt/v%)	Al_2O_3 (wt%)
PS substrate	16	6	2	76.0	0.0			
$PS_{0.5}$ substrate	16	6	2	75.5	0.5			
PS-TFC	16	6	2	76.0	0.0	2	0.1	0.00
$PS_{0.5}$-TFC	16	6	2	75.5	0.5	2	0.1	0.00
$PS_{0.5}$-$TFN_{0.05}$	16	6	2	75.5	0.5	2	0.1	0.05
$PS_{0.5}$-$TFN_{0.1}$	16	6	2	75.5	0.5	2	0.1	0.10

(IP) method with MPD and TMC.[1,13] First, 2 wt% MPD aqueous solution containing 0.1 wt% SDS was poured onto the substrate upper surface and held horizontally at room temperature for 4 min. The excessive MPD solution was removed from the substrate using nitrogen gas, and then, 0.1 w/v% TMC in *n*-hexane solution containing various concentrations of Al_2O_3 nanoparticles, from 0.00 wt% to 0.1 wt%, was poured onto the substrate surface and contacted for 2 min. After removal of excess organic solution, the membrane was oven-dried for 5 min at 80 °C. Finally, the resultant membrane was washed thoroughly with DI water and stored in water base. To distinguish different TFC and TFN membranes, the membrane using PS substrate was denoted as PS-TFC, while the membranes using $PS_{0.5}$ substrate were denoted as $PS_{0.5}$-TFC and $PS_{0.5}$-TFN_x (*x* denotes the concentration (wt%) of Al_2O_3 nanoparticles in PA layer). The synthesis conditions for TFC and TFN membranes are summarized in Table 1. Because the prepared Al_2O_3-based FO membranes exhibited the highest water flux and acceptable solute reverse flux at 0.05 wt% addition of Al_2O_3 nanoparticles in PA layer (Fig. S1†), this loading concentration was selected. Besides, 0.1 wt% loading concentration in PA layer was selected to make a comparison.

2.3 Characterization of Al_2O_3 nanoparticles and membranes

2.3.1 Characterization of Al_2O_3 nanoparticles. The particle size of Al_2O_3 nanoparticles was determined by dynamic light scattering (DLS, Malvern Zetasizer Nano series, UK). To determine the crystal structure of Al_2O_3 nanoparticles, X-ray diffraction (XRD, RigakuD/Max 2200PC) with Cu Kα radiation ($\lambda = 0.15418$ nm) at room temperature with an applied tube voltage and electric current at 40 kV and 20 mA, respectively, was conducted. The Brunauer–Emmett–Teller (BET) theory was used at multiple points to calculate specific surface area and analyze pore size and pore volume of Al_2O_3 nanoparticles. The structure of Al_2O_3 nanoparticles was observed by using a JEM-2100 (JEOL, Japan) working at 200 kV.

2.3.2 Characterization of substrates and FO membranes. It is noted that all membranes were vacuum-dried at 40 °C overnight before characterization. To confirm the surface functional groups, attenuated total refection Fourier-transform infrared spectroscopy (ATR-FTIR, Tensor 27, Bruker, Germany) was applied. By using a scanning electron microscope (SEM, S-4800, Hitachi, Japan), the surface morphology and cross-section of

membranes were analyzed. Notably, the isolated PA layer was separated from the PS support by dissolving PS using dichloromethane. An SEM microscope equipped with an energy-dispersive X-ray (EDX) spectroscope was used to determine elemental compositions of Al_2O_3 nanoparticles and composite membranes. Water contact angle was measured by using an automatic contact angle meter (DSA100, Kruss, Germany) to determine the hydrophilicity of membrane surface. To decrease data error, the measurement was repeated at least six times for each membrane. The membrane surface roughness was detected by *in situ* atomic force microscopy (AFM, Veeco, USA) with tapping mode measurements in air. The scanning area was 2 μm × 2 μm and *Z*-scale was 500 nm. The images showed that surface roughness was denoted as the root mean square (RMS) height. The membrane porosity (ε) was defined as the volume of the pores divided by the total volume of the membrane. It was obtained by gravimetric measurement using the following equation:[18]

$$\varepsilon = \frac{(m_1 - m_2)/\rho_w}{(m_1 - m_2)/\rho_w + m_2/\rho_P} \quad (1)$$

where m_1 (g) and m_2 (g) are wet and dry weights, ρ_w (1.00 g cm^{-3}) is density of water, and ρ_P is density of polymer. It should be noted that the PE mesh was not removed while conducting porosity characterization.

The average pore radius (r_m) of PS substrate and $PS_{0.5}$ substrate could be calculated by the Guerout–Elford–Ferry equation:[30,31]

$$r_m = \frac{\sqrt{(2.90 - 1.75\varepsilon)8\eta h J}}{\varepsilon PS_m} \quad (2)$$

where η is water viscosity (Pa s), J is water flux per unit time, P is operational pressure (0.1 MPa), S_m is effective membrane area, h is membrane thickness and ε is substrate porosity.

2.4 NF and FO performance

2.4.1 Water and solute permeability of substrates and FO membranes. The water and salt permeability of substrates and FO membranes were investigated by using a lab-scale circulating filtration unit to determine permeability and selectivity. The tests were conducted at room temperature with an effective membrane area of 7.065 cm^2. The pure water permeability of PS and $PS_{0.5}$ substrates were investigated using DI water at 1 bar

with a cross-flow rate of 1 L min^{-1}, while the water permeability of TFC and TFN membranes was investigated using DI water at 4 bar. Water flux (J, L m^{-2} h^{-1}) and water permeability coefficient (A, L m^{-2} h^{-1} bar) were calculated using eqn (3) and (4), respectively:[1,29]

$$J = \frac{\Delta V_{feed}}{S_m \Delta t} \quad (3)$$

$$A = \frac{J}{\Delta P} \quad (4)$$

where S_m is effective membrane area, ΔV_{feed} is permeate volume, Δt is measuring time interval and ΔP is trans-membrane pressure difference.

The rejection (R) and solute permeability coefficient (B, L m^{-2} h^{-1}) of TFC and TFN membranes were calculated using feed solution containing 2000 ppm NaCl at 4 bar by eqn (5) and (6), respectively:[32]

$$R = 1 - \frac{C_P}{C_f} \quad (5)$$

$$\frac{1-R}{R} = \frac{B}{A(\Delta P - \Delta \pi)} \quad (6)$$

where C_P and C_f are salt concentrations in the permeate and feed solution, respectively, A is water permeability coefficient, ΔP is pressure difference and $\Delta \pi$ is osmotic pressure difference across the membrane.

2.4.2 Water flux and solute reverse flux of TFC and TFN membranes. FO performance, water flux (J_v, L m^{-2} h^{-1}) and solute reverse flux (J_s, g m^{-2} h^{-1}), was measured by a lab-scale cross-flow set-up with an effective membrane area of 10 cm^2. All FO membranes were tested in two different operational modes: (1) AL-FS where active layer faces the feed solution and (2) AL-DS where active layer faces the draw solution. In the test, DI water and 10 mM NaCl were used as feed solution and 1 M NaCl as draw solution. The solution flow velocities during the tests were kept at 18.5 cm s^{-1} and each experiment lasted for 1 h and was repeated three times to obtain more accurate results. J_v and J_s were determined by measuring the changes in weight and salt concentration in the feed solution, and calculated by eqn (7) and (8):[15]

$$J_v = \frac{\Delta V}{A_m \Delta t} \quad (7)$$

$$J_s = \frac{\Delta(C_t V_t)}{A_m \Delta t} \quad (8)$$

where ΔV is the volume change in feed solution, A_m is effective membrane area, Δt is measuring time interval, and C_t and V_t are salt concentration and volume of the feed solution measured at the end of the time interval, respectively.

Furthermore, the structural parameter (S) of FO membranes can be calculated in accordance with classical internal concentration polarization (ICP) model as expressed in eqn (9):[5]

$$J_v = \frac{D}{S}\left[\ln \frac{A\pi_{draw} + B}{A\pi_{feed} + J_v + B}\right] \quad (9)$$

where J_v is FO water flux, D is solute diffusion coefficient in water, and π_{draw} and π_{feed} are osmotic pressures of the draw and feed solutions, respectively.

In addition, FO performance of PS-TFC, PS$_{0.5}$-TFC and PS$_{0.5}$-TFN$_{0.05}$ membranes was evaluated over a range of NaCl concentrations from 0.5 M to 2 M as draw solution and DI water as feed solution.

2.4.3 Stability of PS$_{0.5}$-TFN$_{0.05}$ membrane. To measure the stability of PS$_{0.5}$-TFN$_{0.05}$ membrane, 80 h long-term FO test was conducted to observe the changes in water flux and solute reverse flux. In addition, PS$_{0.5}$-TFN$_{0.05}$ membrane was stored in an acid solution (pH = 2) and alkali solution (pH = 12) for 7 days, and then the FO test was re-conducted to determine the stability of composite membranes under serious water environment.

3. Result and discussion

3.1 Characterization of Al$_2$O$_3$ nanoparticles

As shown in Fig. 2a, the average size of Al$_2$O$_3$ nanoparticles is 54.7 ± 4.0 nm with a narrow size distribution. The XRD patterns (Fig. 2b) exhibit two relatively strong peaks at 2θ values of about 46.6° and 66.7°, which are attributed to the (400) and (440) reflections of γ-Al$_2$O$_3$ (JCPDS 10-0425), respectively. The other peaks also correspond to the standard card,[33,34] which demonstrated that only γ phase exists in commercial Al$_2$O$_3$ nanoparticles without any other phases such as α and β. It is generally accepted that among the seven transition phases, γ-Al$_2$O$_3$ is the most attractive one for its favorable textural properties (large surface area and high pore volume).[23,35] The structure of Al$_2$O$_3$ nanoparticles is detected by TEM and presented in Fig. 2c. The Al$_2$O$_3$ nanoparticles are spherical and agglomerate to many fine crystallites with sizes ranging from 4 to 6 nm and have a porous structure.[36] The pore diameter of Al$_2$O$_3$ nanoparticles is 5.6 ± 0.7 nm with a relative narrow pore size distribution. In addition, the BET specific surface area is 220 ± 13 m^2 g^{-1} and the pore volume is 0.673 ± 0.055 cm^3 g^{-1} using the Barrett–Joyner–Halenda (BJH) method. The mesoporous structure of commercial Al$_2$O$_3$ nanoparticles makes it an appropriate nanomaterial to serve as a water channel in the fabrication of FO membranes, such as TiO$_2$, SiO$_2$ and MOFs.[19,37] The elemental composition of Al$_2$O$_3$ nanoparticles is shown in Fig. S2.†

3.2 Effect of Al$_2$O$_3$ nanoparticle addition on substrate properties

Fig. 3 displays the surface morphology and cross-section of PS substrate and PS$_{0.5}$ substrate, as well as the distribution of Al element in PS$_{0.5}$ substrate by EDX mapping. We can see that the surface morphology of PS$_{0.5}$ substrate undergoes an obvious change due to incorporation of Al$_2$O$_3$ nanoparticles in the dope solution. The pore size together with the overall porosity of PS$_{0.5}$ substrate both show an increase, as shown in Table 2. Compared to pure PS dope solution, the presence of hydrophilic Al$_2$O$_3$ nanoparticles in the dope solution may strongly facilitate diffusion of water from the water coagulation bath to the cast
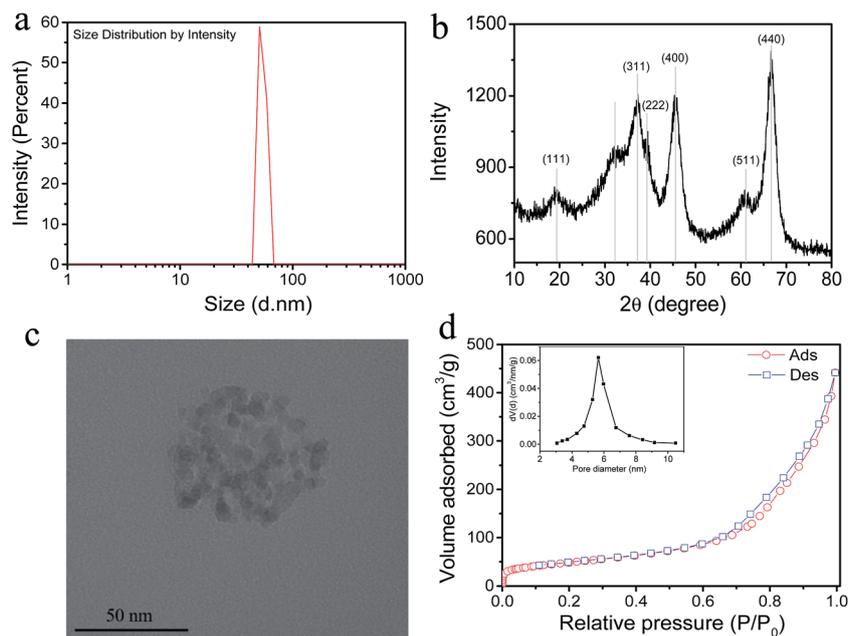
Fig. 2 (a) Average size of Al_2O_3 nanoparticles; (b) XRD patterns of Al_2O_3 nanoparticles; (c) TEM images of Al_2O_3 nanoparticles and (d) nitrogen adsorption–desorption isotherms and pore size distribution curve (inset) of Al_2O_3 nanoparticles.
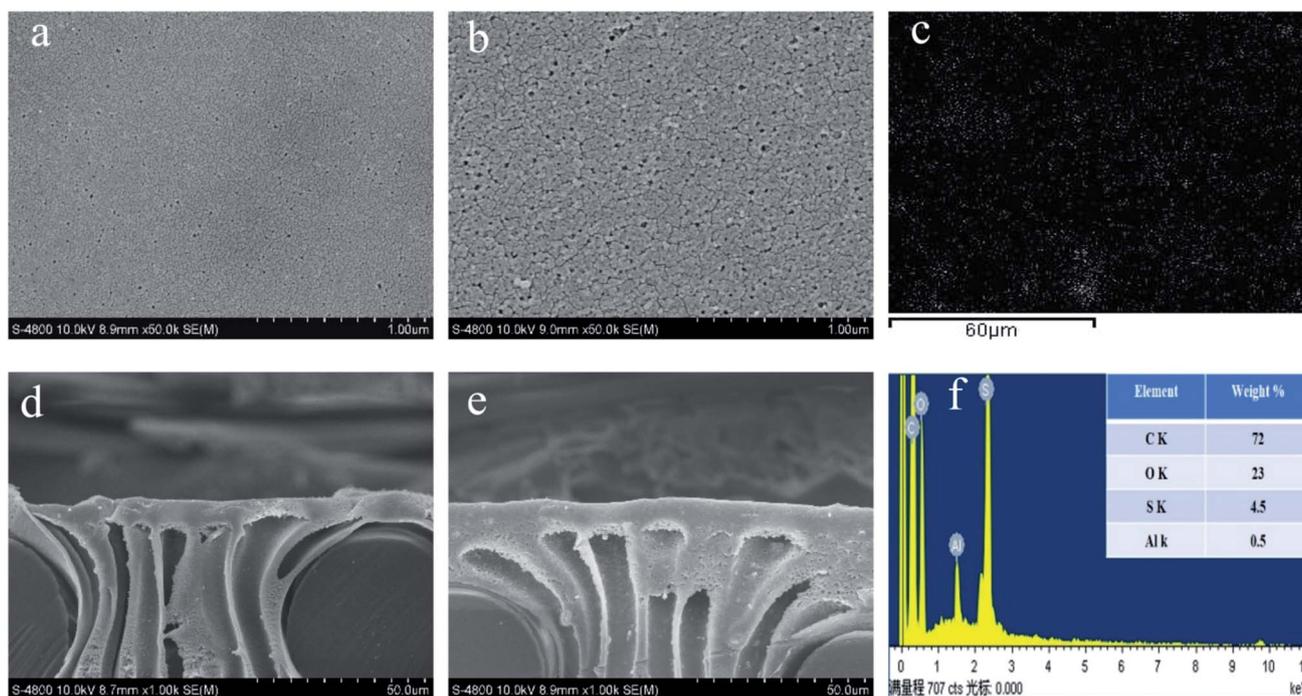

Fig. 3 Surface morphology and cross-section of PS substrate (a) and (d) and $PS_{0.5}$ substrate (b) and (e). EDX mapping image (Al) and composition of $PS_{0.5}$ substrate (c) and (f), respectively.

polymer film, leading to enlargement in overall porosity and pore size of $PS_{0.5}$ substrate.[38] However, little difference is observed in the cross-sectional images of PS and $PS_{0.5}$ substrates, and both comprise a dense layer and a straight finger-like structure. It is acceptable that high porosity associated with finger-like structure of the substrate can cause

minimization of the structural parameter (S) and a small S value unavoidably leads to lower ICP and better FO performance.[17]

EDX mapping results are presented in Fig. 3c. Slight aggregation of Al_2O_3 nanoparticles is detected in the $PS_{0.5}$ substrate, which leads to increase in surface roughness from 20.571 nm for PS substrate to 25.347 nm for $PS_{0.5}$ substrate, as shown in

Table 2 Effect of Al$_2$O$_3$ nanoparticle addition on substrate properties with respect to water permeability, pore size, overall porosity, contact angle surface roughness and structure parameter

Membrane	Pure water permeability (L m^{-2} h^{-1} bar)	Porosity (%)	Pore size (nm)	Contact angle (°)	RMS (nm)	S value (µm)
PS	174 ± 8	63.2 ± 1.7	30.7 ± 0.7	80.4 ± 2.1	20.571	1422
PS$_{0.5}$	261 ± 14	71.1 ± 2.1	34.1 ± 0.9	67.7 ± 2.6	25.347	1028

Table 2. Nevertheless, the water contact angle shows a reduction for the PS$_{0.5}$ substrate, indicating the enhancement in hydrophilicity. During the phase inversion process, the hydrophilic nanoparticles present in dope solution tend to decrease the interface energy, and migrate fast towards to the upper layer of the fabricated membranes. This migration plays a positive role in increasing membrane hydrophilicity, thus decreasing contact angle.[39] Combination of enhanced porosity and hydrophilicity significantly contribute to higher pure water permeability of PS$_{0.5}$ substrate, as presented in Table 2.

3.3 Effect of Al$_2$O$_3$ nanoparticles on FO performance

3.3.1 Surface morphology and surface roughness of FO membranes. Fig. 4 reflects the surface morphology, cross-section and roughness of TFC and TFN membranes. Apparently, the surface of PS-TFC membrane and PS$_{0.5}$-TFC membrane exhibit typical "ridge-and-valley" structure of PA layer with a relatively smooth surface (Fig. 4a, b, e and f).[40] When Al$_2$O$_3$ nanoparticles are added in organic phase, PS$_{0.5}$-

TFN membranes show large "leaf-like" morphological structures, and from the cross-section images, we can observe that their surface has become rougher than that of TFC membranes (Fig. 4g and h). Besides, the isolated PA layer of PS$_{0.5}$-TFN membranes show a slight increase in thickness as compared to TFC membranes. Lind et al.[16] have confirmed that the formation of expanded IP reaction zone induced by enhanced miscibility of aqueous and organic phases upon the addition of hydrophilic nanoparticles plays a vital role in membrane structure. When contacted with the aqueous phase, Al$_2$O$_3$ nanoparticles in organic phase hydrate and then release heat on the IP interface and broaden the reaction zone. Certain amount of MPD molecules may diffuse to broad reaction zone and form large "leaf-like" structures, which resulted in the increase of surface roughness and thickness of the PA layer. When the loading concentration of Al$_2$O$_3$ nanoparticles increases to 0.1 wt%, severe aggregation of Al$_2$O$_3$ nanoparticles is noted in the PA layer with a further increment in surface roughness. The serious aggregation of Al$_2$O$_3$ nanoparticles may induce the formation of macro-voids on the active layer and deteriorate
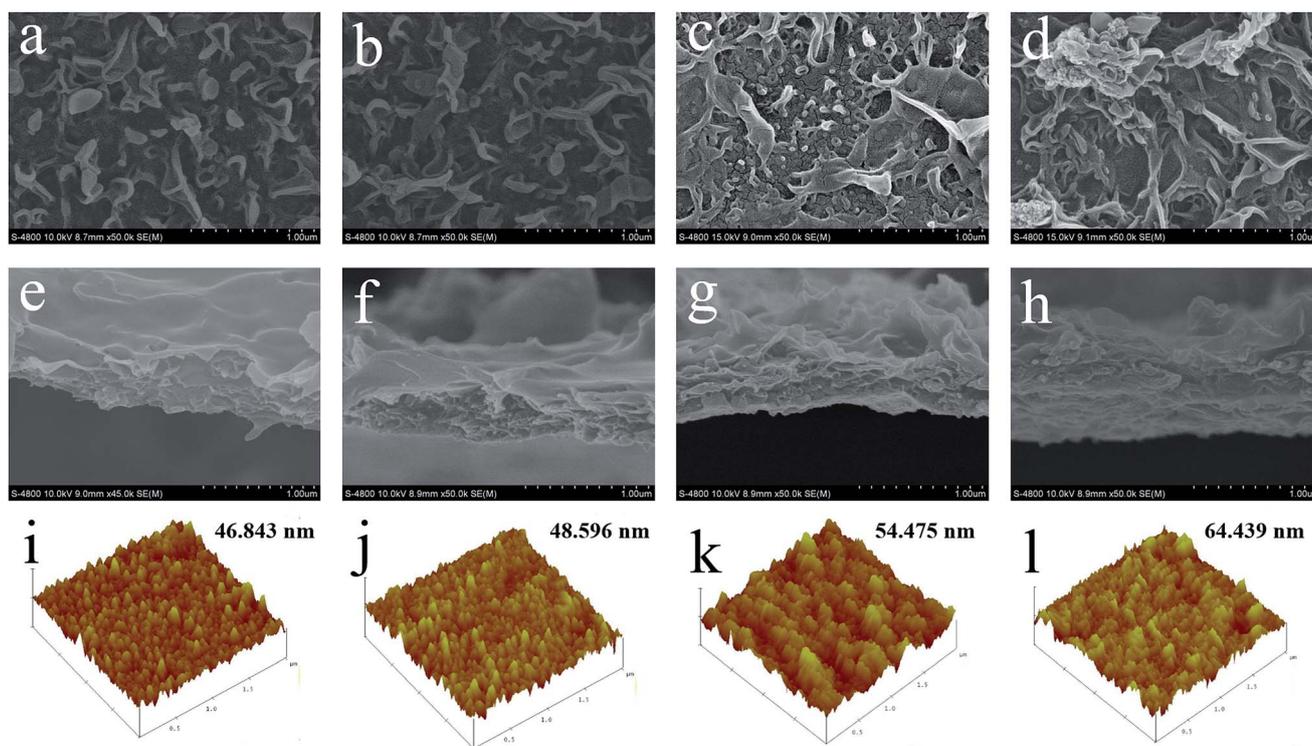

Fig. 4 Surface morphology, cross-section and roughness of TFC and TFN membranes. (a) (e) and (i) PS-TFC membrane; (b), (f) and (j) PS$_{0.5}$-TFC membrane; (c), (g) and (k) PS$_{0.5}$-TFN$_{0.05}$ membrane and (d), (h) and (l) PS$_{0.5}$-TFN$_{0.1}$ membrane (AFM image: scanning scale 2 µm × 2 µm and Z-scale is 500 nm).

structural integrity, thus decreasing salt rejection. Besides, the element composition of TFC and TFN membranes is summarized in Table S1.†

3.3.2 ATR-FTIR spectra and water contact angle of TFC and TFN membranes.

Fig. 5 displays the ATR-FTIR spectra of substrates and FO membranes. For PS and $PS_{0.5}$ substrate, the peaks at 1151 cm^{-1} are attributed to symmetric stretching of O=S=O. The peak at 1240 cm^{-1} and 1400 cm^{-1} represent the asymmetric stretching of C–O–C and aromatic ring stretching of C=C. These peaks correspond to specific functional groups of the substrate made of PS.[1] For TFC and TFN membranes, the typical peaks of PA layer at are detected at 1650 cm^{-1}, 1616 cm^{-1}, and 1487 cm^{-1}, which are attributed to amide I C=O stretching vibrations, hydrogen-bonded C=O stretching vibrations, and amide II N–H bending and torsional motion, respectively.[40] Furthermore, a peak at 831 cm^{-1} representing Al–O stretching vibrations is also observed in $PS_{0.5}$ substrate, $PS_{0.5}$-TFC membrane and $PS_{0.5}$-$TFN_{0.05}$ membrane.[28] These peaks indicate the successful incorporation of Al_2O_3 nanoparticles in both PS substrate and PA layer.

The water contact angle of TFC and TFN membranes is presented in Fig. 5f. Little difference is observed between PS-TFC and $PS_{0.5}$-TFC membranes due to their similar functional groups such as $-NH_2$ and $-COO^-$ on the membrane surface. When Al_2O_3 nanoparticles are incorporated in the PA layer, an obvious decrease in water contact angle is observed for $PS_{0.5}$-TFN membranes. It is agreed that a small contact angle represents high hydrophilicity of membrane surface.[29] The contact angle can be influenced by membrane surface roughness and it is greater on rough solids than on relatively smooth surfaces because of the hysteresis of wetting increases with degree of roughness.[39] However, as shown in Fig. 5f, the contact angle decreases with increase in surface roughness. Prakash et al.[41] have proposed that roughness factor alone does not ensure hydrophilic behavior of membrane surface. Thus, the reduction of contact angle of $PS_{0.5}$-TFN membranes suggest that the incorporation of Al_2O_3 nanoparticles decreases interface energy and develops nano-channels on surfaces, thus allowing easy water-droplet expansion on its surface.[5]

3.3.3 NF performance of TFC and TFN membranes.

Table 3 summarizes the water permeability and solute permeability of TFC and TFN membranes during NF test. As can be seen, $PS_{0.5}$-TFC and $PS_{0.5}$-TFN membranes exhibit an increment in water flux compared to pure PS-TFC membrane, indicating that the incorporation of Al_2O_3 nanoparticles in substrate and PA layer has a positive effect (such as improved hydrophilicity of substrate and PA layer as well as the enlargement of pore size and porosity of substrate) on the enhancement of TFC membrane performance. It must be noted that we obtain a higher water flux and salt rejection of $PS_{0.5}$-$TFN_{0.05}$ membrane compared to the results reported by Saleh et al.,[28] which is attributed to the combined improvement of substrate and PA layer properties. However, when Al_2O_3 nanoparticles addition in PA layer is increased to 0.1 wt%, a sharp increase in solute permeability is noted. This is most probably caused by severe aggregation of Al_2O_3 nanoparticles in the PA layer, thus inducing deterioration of integrity of the PA layer and decreasing salt rejection. The results correspond to SEM images observed in Fig. 4d. The solute permeability/water permeability ratio (B/A ratio) is also presented in Table 3. Multiple studies have reported that the B/A ratio is an important parameter related to membrane selectivity in FO processes, where a small B/A ratio is preferred to reduced solute reverse diffusion.[1,15,37,38] Considering the high water permeability and low B/A ratio, the $PS_{0.5}$-$TFN_{0.05}$ membrane exhibits good potential for FO application.

3.3.4 FO performance of TFC and TFN membranes.

Fig. 6a compares the water flux and solute reverse flux of TFC and TFN membranes using DI water as feed solution and 1 M NaCl as draw solution. Clearly, $PS_{0.5}$-TFC membrane (13.3 L m^{-2} h^{-1}) exhibits higher water flux (13.3 L m^{-2} h^{-1}) than PS-TFC membrane (9.9 L m^{-2} h^{-1}) with slight increase in solute reverse flux. We believe that the enhancement in water flux resulted from substrate property (porosity and hydrophilicity) changes upon the addition of Al_2O_3 nanoparticles in substrate. These changes contribute to the much lower S value of $PS_{0.5}$-TFC membrane than of PS-TFC membrane, as shown in Table 2,
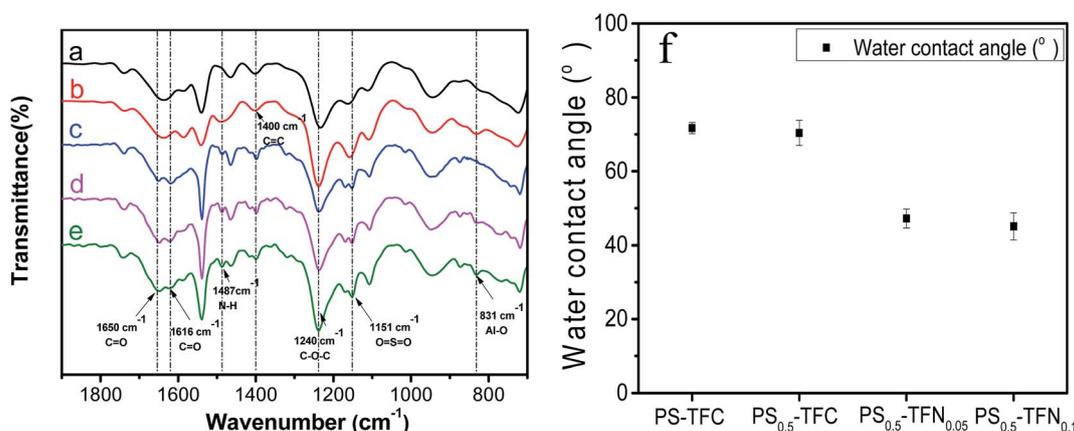

Fig. 5 ATR-FTIR spectra of substrates and FO membranes. (a) PS substrate; (b) $PS_{0.5}$ substrate; (c) PS-TFC membrane; (d) $PS_{0.5}$-TFC membrane; and (e) $PS_{0.5}$-$TFN_{0.05}$ membrane. Water contact angle of TFC and TFN membranes (f).

Table 3 Separation properties of TFC and TFN membranes

Membrane	Water permeability[a] (L m^{-2} h^{-1} bar)	Solute permeability[b] (L m^{-2} h^{-1})	B/A (bar)
PS-TFC	4.03	0.55	0.14
PS$_{0.5}$-TFC	4.95	0.65	0.13
PS$_{0.5}$-TFN$_{0.05}$	8.43	1.66	0.20
PS$_{0.5}$-TFN$_{0.1}$	12.78	21.8	1.66

[a] Water permeability was measured in NF testing mode at 4 bar and DI water as feed solution. [b] Solute permeability was measured in NF testing mode at 4 bar and 2000 ppm NaCl as feed solution.

indicating that Al_2O_3 incorporation in substrate greatly improves mass transfer efficiency of the substrate, thus minimizing transport resistance against water permeation.[10] When Al_2O_3 nanoparticles are incorporated in the PA layer, further enhancement in water flux of PS$_{0.5}$-TFN$_{0.05}$ membrane is observed. The PS$_{0.5}$-TFN$_{0.05}$ membrane shows a water flux of about 27.6 L m^{-2} h^{-1} with slight increase in solute reverse flux. We speculate that the improved water flux of PS$_{0.5}$-TFN$_{0.05}$ membranes was attributed to increased membrane surface roughness (and thus increased polyamide surface area) associated with improved hydrophilicity, which increases the transition rate of water molecules, thus leading to such water flux enhancement.[5,15,17] Besides, the Al_2O_3 nanoparticles may also react as nanochannels in the PA layer. It should be noted that S value discussed here is the apparent value calculated from the flux-fitting method using eqn (9) instead of the intrinsic structural parameter of the substrate. Thus, the calculated apparent S value would be partially influenced by active layer properties, such as A and B values.[42] However, further increase in Al_2O_3 nanoparticles at 0.1 wt% results in a slight enhancement in water flux and high solute reverse flux. The PS$_{0.5}$-TFN$_{0.1}$ membrane no longer possesses selectivity due to severe aggregation of Al_2O_3 nanoparticles and integrity destruction of PA layer. Similar change trends in water flux and solute reverse flux are also detected in AL-DS mode (Fig. S3†). Besides, the water flux and solute reverse flux of PS-TFC membrane, PS$_{0.5}$-TFC membrane and PS$_{0.5}$-TFN$_{0.05}$ membrane using 10 mM NaCl as feed solution

is also conducted and the results are presented in Fig. S4 and Table S2.† From the above results, we observe that instead of simple modification of substrate by addition of nanomaterials in dope solution, incorporation of nanomaterials in both substrate and PA layer may obtain a synergistic enhancement in FO performance and a higher increase in water flux, which is in accordance with the findings reported by Pendergast *et al.*[43]

The FO performance of PS-TFC membrane, PS$_{0.5}$-TFC membrane and PS$_{0.5}$-TFN$_{0.05}$ membrane is evaluated over a range of NaCl concentrations (0.5–2.0 M) and are presented in Fig. 6b. As can be seen, the water flux increases for each membrane with increasing DS concentration due to increased osmotic driving force. However, all membranes show a nonlinear increase in water flux at high NaCl concentration, which is most likely owing to dilutive ICP within the porous substrate. Besides, the large draw solution concentration may induce high salt leakage and thus reduce the overall osmotic driving force across the membrane.[44] Table 4 summarizes the comparison of FO performance between the present work and FO membranes reported in literature. Clearly, we have obtained a higher water flux and acceptable solute reverse flux. This result demonstrates that Al_2O_3 nanoparticles would be a potential nanomaterial to fabricate high performance FO membranes.

3.3.5   Stability of PS$_{0.5}$-TFN$_{0.05}$ membrane. To verify the stability of PS$_{0.5}$-TFN$_{0.05}$ membrane, 80 h FO test is performed in AL-FS and AL-DS modes, and the results are presented in Fig. 7a. As observed, the water flux of PS$_{0.5}$-TFN$_{0.05}$ membrane remains stable with a slight drop after 25 h operation in AL-FS orientation. The good stability of PS$_{0.5}$-TFN$_{0.05}$ membrane suggests that the improved properties of substrate and PA layer effectively minimized the effect of ICP on FO performance, leading to relatively stable water flux. When the membrane is oriented in AL-DS mode, different change trend in water flux is observed. The water flux shows a sharp decline in the first 40 h of FO test. Recently, Wang *et al.*[45] have proposed FO shows more severe water flux decline in AL-DS orientation owing to greater water flux. They point that a minor decrease in bulk concentration difference would result in significant water flux decline. Higher water flux in AL-DS orientation is more susceptible to concentration difference variation, thus showing more severe
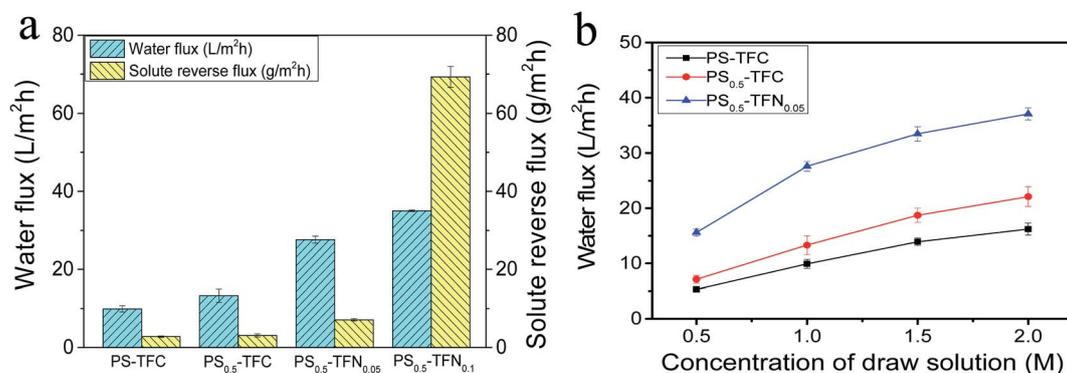

Fig. 6 Water flux and solute reverse flux of PS-TFC membrane, PS$_{0.5}$-TFC membrane, PS$_{0.5}$-TFN$_{0.05}$ membrane and PS$_{0.5}$-TFN$_{0.1}$ membrane (a) (test conditions: DI water as feed solution, 1 M NaCl as draw solution, AL-FS); effect of DS concentration on water flux of PS-TFC membrane, PS$_{0.5}$-TFC membrane, and PS$_{0.5}$-TFN$_{0.05}$ membrane (b) (test conditions: DI water as feed solution, 0.5 to 2.0 M NaCl as draw solution, AL-FS).

Table 4 Comparison of FO performance between present work and FO membranes reported in literature

| FO membrane	J_v (L m^{-2} h^{-1}) AL-FS/AL-DS	J_s (g m^{-2} h^{-1}) AL-FS/AL-DS	FS	DS
TFN membranes by addition of TiO$_2$ on PS substrate[1]	17.1/31.2	2.9/6.66	10 mM NaCl	0.5 M NaCl
CNT incorporated double-skinned TFN membranes[18]	8.3/—	2.7/—	DI water	2 M MgCl$_2$
AqpZ-based lipid membrane through covalent bonding on PS substrate[29]	23.1/—	3.1/—	DI water	2 M MgCl$_2$
MPD–TMC–NaY over PS substrate[15]	16.5/30	9.8/20.0	DI water	1 M NaCl
TFN membrane upon addition of Al$_2$O$_3$ on PS substrate and PA layer (this work)	27.6/51.5	7.1/12.7	DI water	1 M NaCl
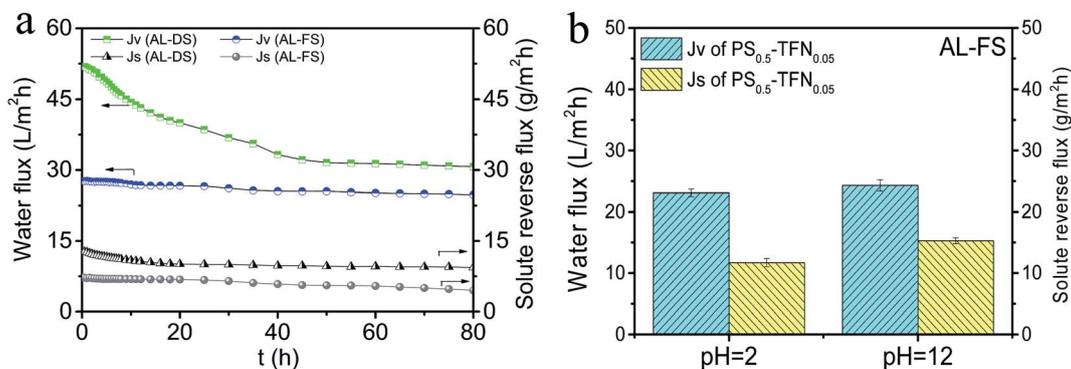
Fig. 7 (a) Water flux and solute reverse flux of PS$_{0.5}$-TFN$_{0.05}$ membrane during 80 h FO test (test conditions: DI water as feed solution, 1 M NaCl as draw solution, AL-FS mode and AL-DS mode); (b) water flux and solute reverse flux of PS$_{0.5}$-TFN$_{0.05}$ membrane after treatment with acid solution (pH = 2) and alkali solution (pH = 12) in AL-FS mode.

water flux decrease during the long-term FO test. Finally, the membranes gain a steady but nearly a half of the initial flux.

Most commercial polyamide TFC membranes allow stable operation within the pH range of 2 to 11. In the present work, we investigate the stability of PS$_{0.5}$-TFN$_{0.05}$ membrane stored in acid solution (pH = 2) and alkali solution (pH = 12) for 7 days. As observed in Fig. 7b, the water flux remains almost unchanged with slight increase in solute reverse flux after treatment of acid and alkali solutions, which demonstrates a highly stable PS$_{0.5}$-TFN$_{0.05}$ membrane. Nonetheless, we need to pay attention to the point that the integrity of PA layer is easily degraded under alkali conditions and the solute reverse flux displays a relative higher increase, which agrees with our previous work.[46]

4. Conclusions

In the present work, hydrophilic nano-sized Al$_2$O$_3$ nanoparticles were used as additives in both substrate and polyamide (PA) active layer to fabricate highly permeable FO membranes. By incorporation of Al$_2$O$_3$ nanoparticles in the substrate, the pore size, overall porosity and hydrophilicity greatly improved, leading to a smaller S value than that of pure PS substrate. Also, by addition of Al$_2$O$_3$ nanoparticles in the PA layer, further enhancement in water flux was achieved. Upon incorporation of 0.5 wt% Al$_2$O$_3$ in the substrate and 0.05 wt% Al$_2$O$_3$ in the PA layer

(PS$_{0.5}$-TFN$_{0.05}$ membrane), the water flux reached 27.6 L m^{-2} h^{-1} with a relatively low solute reverse flux of 7.1 g m^{-2} h^{-1} using DI water as feed solution and 1 M NaCl as draw solution. Compared to the simple incorporation of nanomaterials in substrate, incorporation of nanomaterials in both substrate and PA layer had a better effect on FO performance and a higher water flux was obtained. Besides, the PS$_{0.5}$-TFN$_{0.05}$ membrane remained stable for a long time in FO test and under serious water environment. We believe that nano-sized Al$_2$O$_3$-based FO membranes will have a wide application in the field of water purification.

Conflicts of interest

There are no conflicts to declare.

Acknowledgements

References

1 D. Emadzadeh, W. J. Lau, T. Matsuura, M. Rahbari-Sisakht and A. F. Ismail, *Chem. Eng. J.*, 2014, **237**, 70–80.

2 J. Ren and J. R. McCutcheon, *Desalination*, 2014, **343**, 187–193.

3 Q. Ge, M. Ling and T. S. Chung, *J. Membr. Sci.*, 2013, **442**, 225–237.

4 S. Zhao, L. Zou, C. Y. Tang and D. Mulcahy, *J. Membr. Sci.*, 2012, **396**, 1–21.

5 M. Amini, M. Jahanshahi and A. Rahimpour, *J. Membr. Sci.*, 2013, **435**, 233–241.

6 B. Mi and M. Elimelech, *J. Membr. Sci.*, 2010, **348**, 337–345.

7 G. Han, S. Zhang, X. Li, N. Widjojo and T. S. Chung, *Chem. Eng. Sci.*, 2012, **80**, 219–231.

8 T. S. Chung, X. Li, R. C. Ong, Q. Ge, H. Wang and G. Han, *Curr. Opin. Chem. Eng.*, 2012, **1**, 246–257.

9 T. Cath, A. Childress and M. Elimelech, *J. Membr. Sci.*, 2006, **281**, 70–87.

10 N. Ma, J. Wei, S. Qi, Y. Zhao, Y. Gao and C. Y. Tang, *J. Membr. Sci.*, 2013, **441**, 54–62.

11 J. Su and T. S. Chung, *J. Membr. Sci.*, 2011, **376**, 214–224.

12 A. Tiraferri, N. Y. Yip, W. A. Phillip, J. D. Schiffman and M. Elimelech, *J. Membr. Sci.*, 2011, **367**, 340–352.

13 Z. Zhou, J. Y. Lee and T. S. Chung, *Chem. Eng. J.*, 2014, **249**, 236–245.

14 J. Wei, C. Qiu, C. Y. Tang, R. Wang and A. G. Fane, *J. Membr. Sci.*, 2011, **372**, 292–302.

15 N. Ma, J. Wei, R. Liao and C. Y. Tang, *J. Membr. Sci.*, 2012, **405**, 149–157.

16 M. L. Lind, A. K. Ghosh, A. Jawor, X. Huang, W. Hou, Y. Yang and E. M. Hoek, *Langmuir*, 2009, **25**, 10139–10145.

17 N. Niksefat, M. Jahanshahi and A. Rahimpour, *Desalination*, 2014, **343**, 140–146.

18 X. Song, L. Wang, C. Y. Tang, Z. Wang and C. Gao, *Desalination*, 2015, **369**, 1–9.

19 Y. Xu, X. L. Gao, X. J. Wang, Q. Wang, Z. Y. Ji, X. Y. Wang, T. Wu and C. J. Gao, *Materials*, 2016, **9**(11), 870.

20 S. Lim, M. J. Park, S. Phuntsho, L. D. Tijing, G. M. Nisola, W. G. Shim, W. J. Chung and H. K. Shon, *Polymer*, 2017, **110**, 36–48.

21 P. Lu, S. Liang, L. Qiu, Y. Gao and Q. Wang, *J. Membr. Sci.*, 2016, **504**, 196–205.

22 N. Uzal, N. Ates, S. Saki, Y. E. Bulbul and Y. Chen, *Sep. Purif. Technol.*, 2017, **187**, 118–126.

23 L. Samain, A. Jaworski, M. Edén, D. M. Ladd, D. K. Seo, F. Javier Garcia-Garcia and U. Häussermann, *J. Solid State Chem.*, 2014, **217**, 1–8.

24 L. Yan, Y. Li, C. Xiang and S. Xianda, *J. Membr. Sci.*, 2006, **276**, 162–167.

25 Z. Wang, Y. M. Wei, Z. L. Xu, Y. Cao, Z. Q. Dong and X. L. Shi, *J. Membr. Sci.*, 2016, **503**, 69–80.

26 S. Hartmann, A. Sachse and A. Galarneau, *Materials*, 2012, **5**, 336–349.

27 R. Bleta, P. Alphonse, L. Pin, M. Gressier and M. J. Menu, *J. Colloid Interface Sci.*, 2012, **367**, 120–128.

28 T. A. Saleh and V. K. Gupta, *Sep. Purif. Technol.*, 2012, **89**, 245–251.

29 W. D. Ding, J. Cai, Z. Y. Yu, Q. H. Wang, Z. N. Xu, Z. N. Wang and C. J. Gao, *J. Mater. Chem. A*, 2015, **3**, 20118–20126.

30 J. Garcia-Ivars, M. I. Alcaina-Miranda, M. I. Iborra-Clar, J. A. Mendoza-Roca and L. Pastor-Alcañiz, *Sep. Purif. Technol.*, 2014, **128**, 45–57.

31 E. Yuliwati, A. F. Ismail, T. Matsuura, M. A. Kassim and M. S. Abdullah, *Desalination*, 2011, **283**, 214–220.

32 S. Zhang, P. Liu, Y. Chen, J. Jin, L. Hu and X. Jian, *Chem. Eng. Sci.*, 2017, **166**, 91–100.

33 F. Wang, J. P. Lin, Y. F. Liang, S. L. Shang and Z. K. Liu, *Mater. Des.*, 2016, **109**, 700–708.

34 L. Qin, Y. Zheng, D. Li, Y. Zhou, L. Zhang and Z. Zuhra, *Fuel*, 2016, **181**, 827–835.

35 S. Wang, X. Li, S. Wang, Y. Li and Y. Zhai, *Mater. Lett.*, 2008, **62**, 3552–3554.

36 L. Zhu, S. Pu, K. Liu, T. Zhu, F. Lu and J. Li, *Mater. Lett.*, 2012, **83**, 73–75.

37 A. Zirehpour, A. Rahimpour and M. Ulbricht, *J. Membr. Sci.*, 2017, **531**, 59–67.

38 D. Emadzadeh, W. J. Lau and A. F. Ismail, *Desalination*, 2013, **330**, 90–99.

39 S. Zinadini, S. Rostami, V. Vatanpour and E. Jalilian, *J. Membr. Sci.*, 2017, **529**, 133–141.

40 L. Liu, G. Zhu, Z. Liu and C. Gao, *Desalination*, 2016, **394**, 72–82.

41 C. G. Jothi Prakash, C. Clement Raj and R. Prasanth, *J. Colloid Interface Sci.*, 2017, **496**, 300–310.

42 X. Liu and H. Y. Ng, *J. Membr. Sci.*, 2015, **481**, 148–163.

43 M. M. Pendergast, A. K. Ghosh and E. M. V. Hoek, *Desalination*, 2013, **308**, 180–185.

44 G. Han, T. S. Chung, M. Toriida and S. Tamai, *J. Membr. Sci.*, 2012, **423–424**, 543–555.

45 Q. Wang, X. L. Gao, Y. S. Zhang, J. Wang, Y. Xu, Z. Y. Ji, X. Y. Wang and C. J. Gao, *Chem. Eng. Res. Des.*, 2017, **117**, 593–603.

46 K. P. Lee, J. Zheng, G. Bargeman, A. J. B. Kemperman and N. E. Benes, *J. Membr. Sci.*, 2015, **478**, 75–84.